iScience

CellPress
OPEN ACCESS

Article

Zika virus exists in enterocytes and enteroendocrine cells of the *Aedes aegypti* midgut

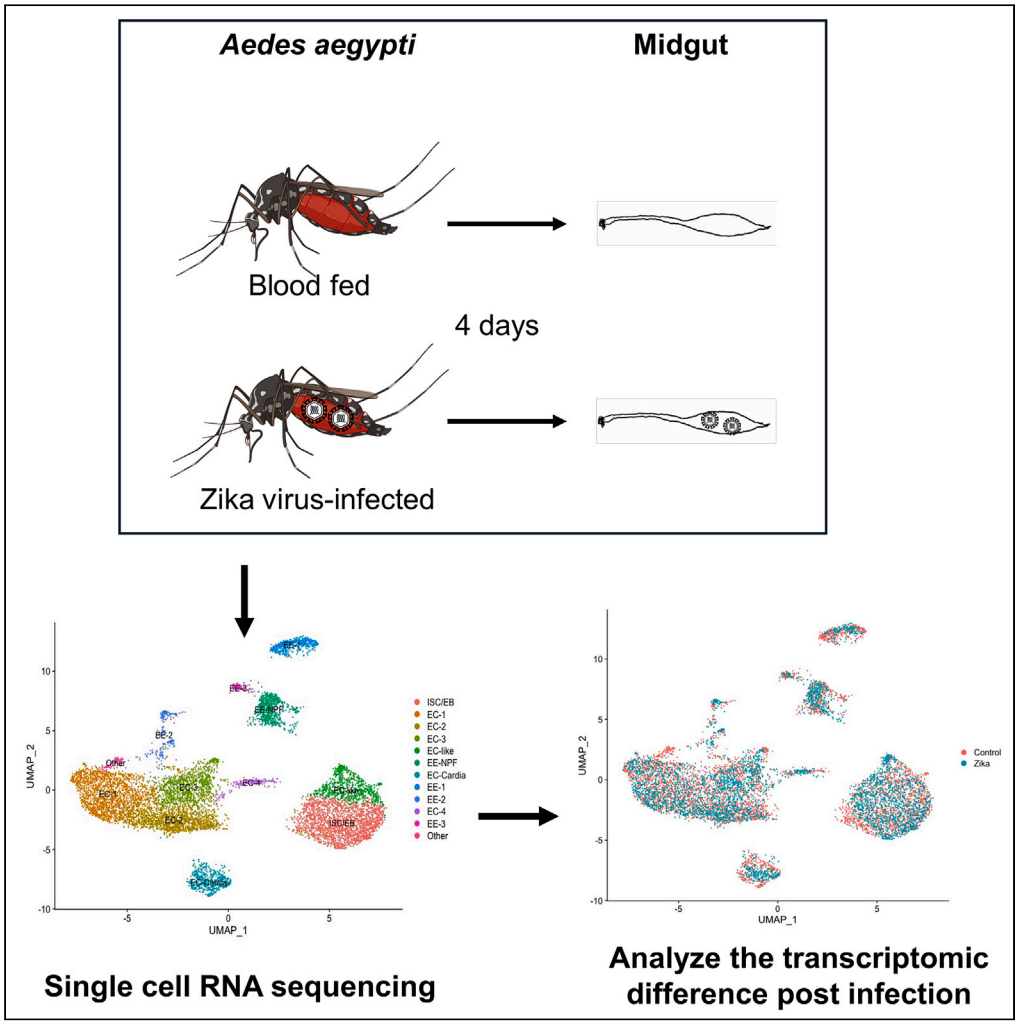

Tse-Yu Chen, Hamidah Raduwan, Alejandro Marín-López, Yingjun Cui, Erol Fikrig

tse-yu.chen@yale.edu

Highlights

Identified distinct cell clusters in *Ae. aegypti* midgut post-Zika virus infection

Virus detected in specific enterocytes and enteroendocrine cell subsets

Significant transcriptomic changes in each cell subset post-infection

Silencing apolipophorin III reduced Zika virus RNA in midgut

Chen et al., iScience 27, 110353
July 19, 2024
https://doi.org/10.1016/j.isci.2024.110353

iScience

CellPress
OPEN ACCESS

Article

Zika virus exists in enterocytes and enteroendocrine cells of the *Aedes aegypti* midgut

Tse-Yu Chen,[1,2,*] Hamidah Raduwan,[1] Alejandro Marín-López,[1] Yingjun Cui,[1] and Erol Fikrig[1]

SUMMARY

The *Aedes aegypti* midgut is crucial for blood digestion, nutrition, reproduction, and pathogen interaction. Using single-cell RNA sequencing, we explored virus infection and transcriptomic changes at the cellular level. We identified 12 distinct cell clusters in the *Ae. aegypti* midgut post-Zika virus infection, including intestinal stem cells, enteroblasts, enteroendocrine cells (EE), and enterocytes (ECs). The virus was found mainly in specific subsets of ECs and EE. Infection altered transcriptional profiles related to metabolism, signaling, and immune responses. Functional studies highlighted three significantly differentially expressed genes in infected cells. Notably, silencing apolipophorin III reduced virus RNA copy number in the midgut, emphasizing the role of specific genes in viral infection. These findings enhance our understanding of mosquito midgut cell processes during Zika virus infection and suggest potential targets for vector control.

INTRODUCTION

The adult mosquito midgut is comprised of a single-layered epithelium surrounded by basal lamina that contains fibrous extracellular matrix.[1] The midgut tissue encompasses various cell types with distinct functions, including digestion, nutrient absorption, and hormone production.[2] It is the primary site for the initial encounter with external pathogens, representing a critical tissue that is susceptible to arbovirus infection.[3] The vector competence of a mosquito during systemic arbovirus infection is significantly influenced by both the midgut infection barrier and the midgut escape barrier.[4] The early phase of the viral replication cycle in the midgut holds paramount importance in shaping the course of infection and ultimately determining the mosquito's competence to transmit the virus.[5]

Four major cell types have been described in both mosquitoes and Drosophila: intestinal stem cells (ISC), enteroblasts (EBs), enterocytes (ECs), and enteroendocrine cells (EE).[6,7] The regulation of ISC proliferation and differentiation involves distinct signaling pathways, contributing to homeostasis and regeneration. ISC proliferation is stimulated by the Hippo, Janus kinase/signal transducers and activators of transcription (JAK-STAT), and epidermal growth factor receptor (EGFR) pathways,[8–10] while ISC differentiation is regulated by the Notch signaling pathway.[11] To maintain homeostasis, ISC undergoes asymmetric division, giving rise to a transient progenitor, the EB, which subsequently differentiates into either EC or EE.[12] The ISCs produce the Notch ligand *Delta*, initiating a Notch-dependent pathway in the EB, thereby driving its differentiation into EC. In the absence of Notch signaling, there is an expansion of Delta-positive proliferative stem-like cells and EE.[12–14] These differentiated cells play a crucial role in replenishing the cellular pool during growth, development, or in response to injury.[13,15] Additionally, both ISC and EB express the Snail family zinc-finger transcription factor *escargot*, contributing to the maintenance of stemness and suppression of differentiation.[13,16] The EB is characterized by the transient expression of the WT-1 like transcription factor *Klumpfuss*, which plays a regulatory role in the differentiation process following Notch activation.[6,17]

The ECs, which predominantly constitute the cellular population, play a key role by secreting digestive enzymes and facilitating the absorption and transport of nutrients. In addition to expressing *trypsin*, the *Nubbin/POU domain protein 1* (*Pdm1*) is identified as an enterocyte marker, with high expression in mature ECs.[6,18,19] The transcriptional factor *Prospero* regulates the commitment of ISC to EE.[20] The EE functions as chemosensory cells, crucial in regulatory activities through neuropeptide/peptide hormone production and secretion. Various gut hormone peptides, including *neuropeptide F* (NPF),[21] the *Allatostatins* family,[22] *tachykinins*,[23] and others,[24] exert influence on diverse physiological processes. Additionally, gustatory receptors in EE may contribute to their chemosensory functions.[25]

To further explore and characterize the gene expression and cell types in the mosquito midgut, we employed single-cell RNA sequencing (scRNA-seq).[26] This approach offers an unbiased method to explore cell-type diversity, function, and establish relationships between different cell types and the virus. Importantly, to accurately detect the virus status in each cell, we isolated entire live midgut cells for the scRNA-seq analysis. Specifically, we chose to focus on the *Ae. aegypti* midgut four days following Zika virus infection, a time point that has been reported

[1]Section of Infectious Diseases, Department of Internal Medicine, School of Medicine, Yale University, New Haven, CT 06520, USA
[2]Lead contact
*Correspondence: tse-yu.chen@yale.edu
https://doi.org/10.1016/j.isci.2024.110353

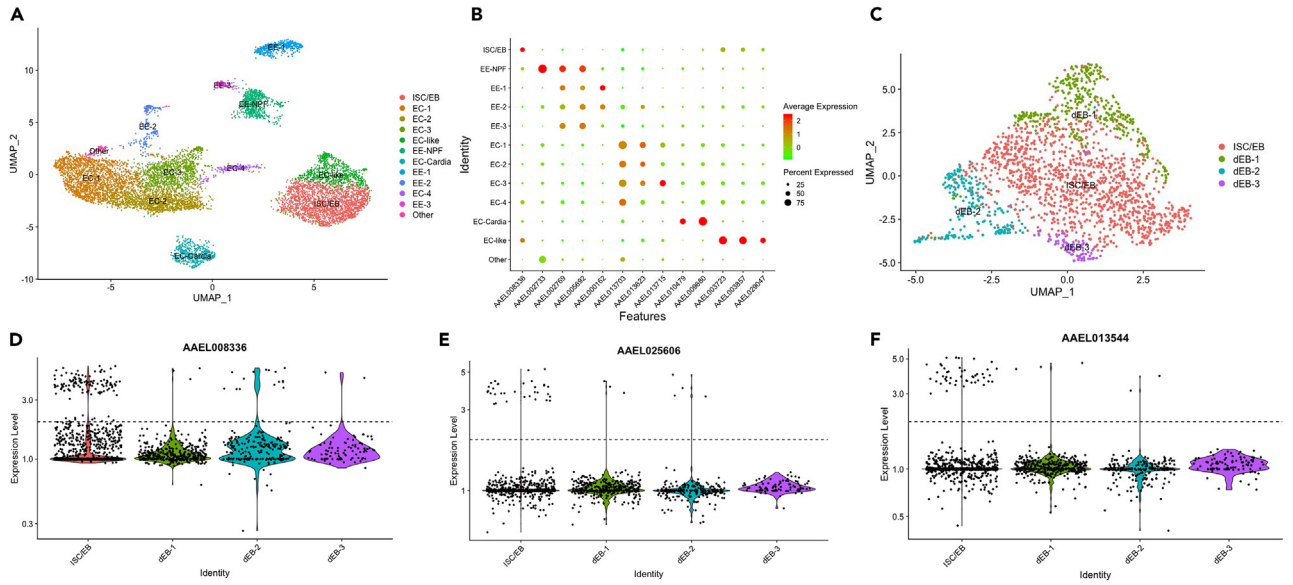

Figure 1. Single-cell RNA sequencing identifies 12 cell clusters in the female *Ae. aegypti* midgut with a total 9345 cells

(A) Annotated cell types visualized on the UMAP of 9345 cells.

(B) Dot plot depicting expression levels and the percentage of cells expressing markers in each cluster.

(C–F) Subclusters derived from the intestinal stem cell/enteroblasts (ISC/EB) cluster with a total 1956 cells. (C) Annotated cell types visualized on the UMAP subdivided into 4 subclusters. Expression of the marker genes (D) *snail* (AAEL008336), (E) *Delta* (AAEL025606), (F) *Klumpfuss* (AAEL013544) in the ISC/EB, dEB-1, dEB-2, and dEB-3 subcluster. Marker genes were represented on a log scale and a dashed line indicated a fold-change of 2.

to have higher infection rates to flavivirus.[27] This period is crucial for determining whether the virus can successfully escape from the midgut.[5] Our study unveils the first evidence of virus presence in both EC and EE, suggesting a potential preference for specific cell targets in virus infection. Furthermore, we showcase the transcriptomic differences at the cellular level following Zika virus infection, illustrating the intricate interactions between various cell types and the virus. The identification of significant genes difference between cell type and infection provides potential targets for developing new control strategies and enhances our understanding of the cellular responses within the mosquito midgut during Zika virus infection.

RESULTS

Unbiased scRNA-seq analysis identified 12 distinct clusters in the female adult *Ae. aegypti* midgut

We utilized the 10x Genomic platform to profile the transcriptome of single midgut epithelial cells obtained from female *Ae. aegypti*, which were either blood-fed (control) or infected with Zika virus (Zika). The scRNA-seq was performed on 5,454 cells from the control group and 3,891 cells from the Zika group, four days after feeding. We obtained a total of 32,993,386 sequence reads from the midgut cells of control mosquitoes and 29,144,307 sequence reads from the midgut cells of Zika-infected mosquitoes. The average mean read count per cell was 9,294 for the control group and 4,526 for the Zika group. In the control group, we detected a total of 10,958 genes, while in the Zika group, we identified 9,425 genes annotated from the *Ae. aegypti* genome.

Seurat's canonical correlation analysis was used to align the dataset from control and Zika mosquito midgut cell, and then employed to detect variable genes, execute linear dimension reduction, ascertain statistically significant components, and generate clusters. The integrated dataset unveiled 12 discrete clusters that can be visualized through a UMAP plot (Figure 1A). Each cluster was assigned to a specific cell type based on established marker genes from a previous study or referencing *Drosophila* midgut cells.[6,7] (Figure 1B).

One cluster, ISC and EB (ISC/EB), was based on the expression of *snail* (AAEL008336) (Figure 1B). Four clusters were categorized as EE due to the marker gene *Prospero* (AAEL002769) and *IA-2* (AAEL005692) (Figures 1B and S1A–S1F).[6] Among the EE clusters, one particularly exhibited high expression of NPF(AAEL002733) and was denoted as EE-NPF (Figures 1B and S1C).

The EC were represented by four distinct clusters expressing different trypsin-related genes such as *trypsin* (AAEL013703 and AAEL013623), *serine-type endopeptidase* (AAEL013715), and *trypsin 3A1 precursor* (AAEL007818) (Figures 1B and S2A–S2D). A specific cluster expressed *chymotrypsin* (AAEL009680) which is a marker for ECs and a *sugar transporter* (AAEL010479), characteristic of the cardia cell.[7] Therefore, the cluster was named EC-cardia (Figures 1B, S3A, and S3B). The EC marker gene *Nubbin/Pdm1* (AAEL017445) was markedly expressed in the EC-1, EC-2, EC-3, and EC-cardia clusters (Figure S2E). Another cluster exhibited expression in various immune-related genes such as *C-type lysozyme* (AAEL003723), *defensins* (AAEL003857 and AAEL003832), and *cecropin* (AAEL029047) (Figures 1B and S4A–S4D). Though lacking trypsin-related gene expression, we hypothesized they correspond to ECs based on the immune gene expression and named them EC-like cells.[6] While one cluster was in close proximity to ECs based on the UMAP coordinates but did not match any markers from

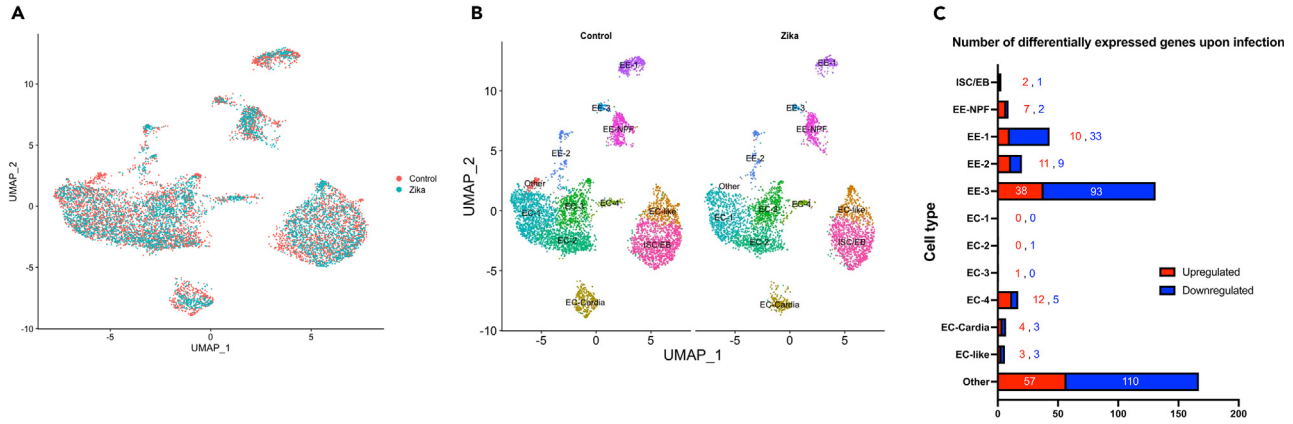

Figure 2. Differences between the midguts of blood-fed and Zika virus-infected mosquitoes

(A) UMAPs from midgut cells of blood-fed (Control, in red, 5454 cells) and Zika virus-infected (Zika, in blue, 3891 cells) mosquitoes.

(B) UMAP with cell type-specific labeling from the control group (left) and Zika group (right).

(C) Number of differentially expressed genes in each midgut cell cluster due to virus infection. Fold-change ≥2 or ≤ -2 and adjusted *p* value <0.05.

previous studies.[7] This cluster expressed one trypsin (AAEL013703), the presence of cells expressing it and the absence of other typical EC gene markers (Figure 1B). Consequently, we designated this cluster as "others", following the naming convention used in a Drosophila midgut study,[6] which identified a "others" cluster involved in metabolism but not classified as ECs.

In our dataset, the ISC/EB cluster demonstrated an indistinguishable profile between ISC and EB, affirming results observed in previous studies of the *Ae. aegypti* and *Drosophila* midguts.[6,7] Nevertheless, to delve deeper into the distribution of ISC and EB, we subdivided the ISC/EB cluster into four distinct subgroups based on their gene expression profiles (Figure 1C). Notably, *snail* (AAEL008336) was predominantly expressed in one of these subgroups (Figure 1D). Furthermore, this subgroup exhibited high expression of both the ISC cell marker gene *Delta* (AAEL025606) and the EB marker gene *Klumpfuss* (AAEL013544) (Figures 1E and 1F). Consequently, we named this subgroup ISC/EB, indicating a highly similar transcriptome for ISC and EB. In contrast, the other three subgroups displayed low levels of ISC and EB marker genes, leading to their classification as differentiating EB (dEB).

Gene expression signatures of each cluster

The cell type markers were employed to analyze the gene expression signature of each cluster using the gProfiler program for Gene Ontology (GO) enrichment analysis.[28] Subsequently, the GO terms were refined through REVIGO to identify specific groups of genes associated with distinct cellular processes.[29] Several common pathways emerged across all clusters, including genes related to translation activity, transcription function, proton transmembrane transporter activity, peptide, and amide biosynthetic processes (Table S2). The ISC/EB cluster exhibited no additional unique GO functions aside from those associated with the Notch pathway and previously mentioned markers (Figures 1E, 1F, and S1). In the EE clusters, in addition to the heightened expression of marker genes, several gut hormone peptides showed varying levels in different EE clusters (Figures S1A–S1F). The *NPF* was highly expressed in EE-NPF, *Preproallatostatin* (AAEL021174) significantly existed in the EE-2 cluster, and *Neurokinin/Tachykinin* (AAEL008282) showed expression across all EE clusters. The *Gustatory receptor* (AAEL000162) was highly expressed in both EE-1 and EE-2 clusters. Besides these specific EE-related transcripts, genes involved in cellular homeostasis were also enriched (Table S3). Within the EC clusters, genes related to the generation of precursor metabolites, ATP metabolic processes, protein folding and maturation, as well as various metabolic and biosynthetic processes (carbohydrate, nucleotide, organophosphate, and small molecules) were prominently enhanced (Table S4). Notably, the EC-cardia cluster exhibited significant gene expression related to the response to toxic substances and detoxification functions (Table S5). The immune response, particularly to bacteria, was highly enriched in the EC-like cluster (Table S6). The cluster named "Others" uniquely expressed cytoplasmic translation functions (Table S7).

The response of Zika virus infection in the midgut of *Ae. aegypti*

The composition of midgut cell types was altered after virus infection (Figures 2A and 2B). Two clusters showed significant changes in cell composition from calculating in Fisher's exact test. (Table 1). The EE-1 cluster decreased from 6.45% in control to 3.60% in Zika (p = 0.004), and the "Others" cluster exhibited a substantial decrease in Zika with only 0.21% compared to 1.89% in the control (p = 0.0002). The remaining ten clusters did not show marked differences between virus-infected and uninfected conditions.

The proportion of subdividing cell types was calculated from on the ISC/EB cluster, and the percentage was determined. (Table 2). All four subclusters exhibited significant differences between the control and Zika conditions. The ISC/EB subcluster showed a decrease in Zika, with only 35.94% compared to 87.44% in the control ($p < 0.0001$). The dEB-1 subcluster displayed higher percentages in Zika, comprising 37.22% as opposed to 4.64% in the control ($p < 0.0001$). Similarly, the dEB-2 subcluster demonstrated a similar trend, accounting for 6.37% in the control and 18.09% in Zika ($p < 0.0001$), while the dEB-3 subcluster exhibited 1.55% in the control and 8.75% in Zika ($p < 0.0001$).

Table 1. The 12 identified cell clusters and their respective percentages in the female *Ae. aegypti* midgut

Cell type	Control (%)	Zika (%)	*p* value
ISC/EB	20.15	22.03	$p = 0.32$
EE-NPF	6.77	7.40	$p = 0.66$
EE-1	6.45	3.60	$p = 0.004$
EE-2	2.53	2.96	$p = 0.58$
EE-3	1.50	0.98	$p = 0.42$
EC-1	20.13	18.30	$p = 0.33$
EC-2	16.19	16.40	$p = 0.95$
EC-3	10.05	12.52	$p = 0.1$
EC-4	1.63	2.26	$p = 0.33$
EC-Cardia	5.61	5.17	$p = 0.77$
EC-like	7.10	8.20	$p = 0.4$
Other	1.89	0.21	$p = 0.0002$

Fisher's exact test was used to calculate the *p* value.

Zika infection also influenced the transcriptomes of most cell types. Under the condition of fold-change ≥ 2 or ≤ -2 and adjusted *p* value <0.05, we observed gene expression differences between control and Zika in all clusters except EC-1 (Figure 2C). In the ISC/EB cluster, two transcripts were upregulated, and one was downregulated after virus infection (Table S8). Notably, *myo-inositol monophosphatase* (AAEL000372), crucial in maintaining intracellular levels of myo-inositol related to several secondary messengers,[30] was decreased in ISC/EB clusters from the Zika group.

Seven genes were increased, and two genes were decreased in the EE-NPF cluster. Two genes related to lipid transport or metabolism—*diazepam binding inhibitor* (AAEL009214)[31] and *apolipophorin III* (AAEL008789)[32,33]—were increased after virus infection (Table S8). In the EE-1 cluster, ten genes were upregulated, and thirty-three genes were downregulated. *Apolipophorin III* also showed an increase in the EE-1 cluster, along with some genes possibly related to extracellular matrix remodeling, such as *matrix metalloproteinase* (AAEL002661),[34] and *fibulin* (AAEL000549).[35] Interestingly, the *neuroendocrine convertase* (AAEL014523), associated with prohormones cleavage,[36] was downregulated in the EE-1 cluster after virus infection (Table S8).

Eleven genes displayed an increase, and nine genes decreased in the EE-2 cluster. The EE marker gene *Prospero* was upregulated in this cluster. We also noticed that one of the G-protein-coupled receptors related to the *myosuppressin* family (AAEL006283) increased, while the *C-type lectin-18* (AAEL005482) decreased their expression under virus infection in the EE-2 cluster (Table S8). The EE-3 cluster exhibited the most significant transcript difference among all the EE clusters with thirty-eight upregulated and ninety-three downregulated genes. Most of the significant genes were related to cellular processes and transporter activity. Particularly, *NPF* was significantly increased in the EE-3 cluster. Additionally, we observed that *C-type lectin mannose binding* (AAEL000543) and one type of *defensin* (AAEL003857) were upregulated under infection (Table S8). Few transcript differences were observed between control and Zika in the EC clusters (Figure 3C). The *metalloproteinase* (AAEL01416) was the only gene that showed a difference in the EC-2 cluster. In the EC-4 cluster, twelve genes increased, and five genes decreased, with the upregulation of *matrix metalloproteinase*. Notably, one of the antimicrobial peptides, *Gambicin* (AAEL004522), was increased in Zika group (Table S8). The EC-cardia clusters exhibited significant differences in seven genes. Two genes associated with digestion, *L-lactate dehydrogenase* (AAEL012014) and *alpha-glucosidase* (AAEL004369), altered their expression. Additionally, *NPF* demonstrated a marked decrease in the EC-Cardia cluster (Table S8). In the EC-like cluster, three transcripts were upregulated, and three were downregulated. The antimicrobial peptide *cecropin* (AAEL029047) significantly increased after virus infection (Table S7). The cluster named "Others" showed the most differences in gene expression levels between control and Zika, with fifty-seven increased and one hundred-ten decreased. Most of the genes were involved in basic biological and cellular processes, as well as the polyol biosynthetic process. Interestingly, we observed a significant increase in the *leucine-rich immune protein* (AAEL010656) in this cluster (Table S8).

Table 2. The 4 identified cell subclusters and their respective percentages, divided from the ISC/EB cluster

Cell type	Control (%)	Zika (%)	*p* value
ISC/EB	87.44	35.94	$p < 0.0001$
dEB-1	4.64	37.22	$p < 0.0001$
dEB-2	6.37	18.09	$p < 0.0001$
dEB-3	1.55	8.75	$p < 0.0001$

Fisher's exact test was used to calculate the *p* value.

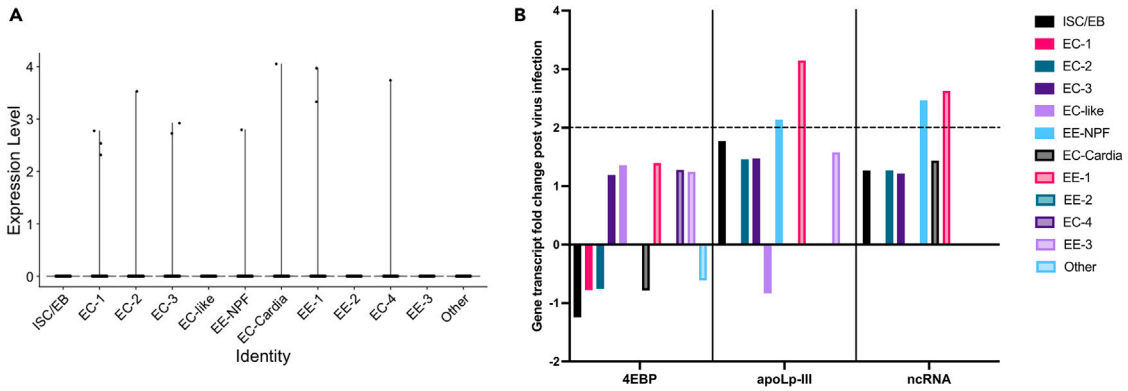

Figure 3. Analysis of Zika virus RNA in mosquito midgut cells

(A) The expression of Zika virus in eleven cells from various cell clusters obtained from Zika-infected mosquito midgut cells, represented in a single-cell violin plot.
(B) The gene expression level changes for the three genes associated with the clusters containing viral RNA: the *eukaryotic translation initiation factor 4E binding protein* (*4EBP*) in enterocyte clusters, and *Apolipophorin III* (*apoLP-III*) and ncRNA in EE-1 and EE-NPF clusters. A dashed line indicated a fold-change of 2.

Zika virus infection in enterocytes and enteroendocrine cells of *Ae. aegypti* midgut

To identify the cell type infected with virus, we sequenced whole live cells isolated from the midgut. The results identified eleven cells contained Zika virus RNA existed in seven clusters, which belonged to either EC (EC-1, EC-2, EC-3, EC-4, and EC-Cardia) or EE (EE-NPF and EE-1) cells (Figure 3A). To identify common gene alterations in infected clusters, we utilized transcriptomic data to compare between clusters (Figure 3B; Table S8). The five EC clusters that detected the virus did not share the same genes from the list of differences between control and Zika under the condition of fold-change ≥ 2 or ≤ -2 and adjusted p value <0.05. If the condition includes only a significance threshold of $p < 0.05$ without considering fold-change, the *eukaryotic translation initiation factor 4E binding protein* (*4EBP*) (AAEL001864) emerges as a significant factor. The *4EBP* showed a different expression pattern among all five EC clusters, being downregulated in EC-1 (fold-change = −1.28), EC-2 (fold-change = −1.33), and EC-cardia (fold-change = −1.27), while upregulated in EC-2 (fold-change = 1.19) and EC-3 (fold-change = 1.28). Two genes overlapped between EE-NPF and EE-1 with a significant increase. The *apolipophorin III* (*apoLP-III*) had a fold-change of 3.14 in the EE-1 cluster and 2.13 in the EE-NPF cluster. The other transcript, one of the ncRNA (AAEL026403), showed a 2.62-fold change in the EE-1 cluster and a 2.46-fold change in the EE-NPF cluster.

Silencing *apolipophorin III* resulted in a decreased RNA copy number of Zika virus in the *Ae. aegypti* midgut

The apoLP-III was selected to validate the impact of Zika virus infection due to its significant upregulation among the virus RNA contained EE clusters. Female *Ae. aegypti* mosquitoes were microinjected with double-strand RNA (dsRNA) targeting either *GFP* or *apoLP-III*. Midgut samples were collected at 2- and 4-day post-virus infection. The knockdown efficiency reached 83% in the mosquito midgut after 2 days of infection ($p < 0.0001$) (Figure 4A). No significant difference was observed between dsGFP and dsapoLP-III in virus RNA copy number at 2 days post-infection ($p = 0.5891$) (Figure 4B). At day 4 post-infection, the knockdown efficiency remained at 85% ($p < 0.0001$) (Figure 4A), and silencing *apoLP-III* resulted in a decreased virus RNA copy number in the midgut ($p = 0.0351$) (Figure 4B). There was no difference in infection prevalence at day 4 post-infection between the two groups (76 ± 13% in dsGFP and 68.5 ± 18.5% in dsapoLP-III).

DISCUSSION

The mosquito midgut, vital for processing nutrients, hormone signaling, and supporting female fecundity, plays a critical role in determining the vector's competence for arboviruses. While previous transcriptomic studies have focused on the midgut at different time points after virus infection, aiming to unravel infection dynamics and identify potential targets for interference, they have operated primarily at the tissue level, examining the entire midgut.[37–39] In contrast to bulk RNA-seq, where average gene expressions are measured across a large cell population, potentially missing nuanced information, scRNA-seq allows for the quantification of the transcriptome of individual cells, providing more detailed and precise information. In this study, we employed scRNA-seq to compare the transcriptomes of individual midgut cells after virus infection. Our findings provide the first evidence of virus presence in both EC and EE, hinting at a potential preference for specific cellular targets in virus infection. Furthermore, in functional studies, we identified three genes significantly differentially expressed among the infected cell clusters. Silencing *apolipophorin III*, one of these genes, resulted in a decreased virus RNA copy number in the midgut, emphasizing the role of specific genes in viral infection as revealed by our scRNA-seq study.

Following the established analysis protocol and gene markers, we successfully identified the major cell types, including ISC, EB, EC, and EE (Figure 1). The 12 clusters identified in our results had fewer cluster numbers compared to the previous study,[7] which revealed less EE clusters but more EC-like and cardia clusters. This discrepancy is possibly due to variations in collecting time points post blood feeding and differences in the isolation method between whole cells and nuclei. The different collection method might also explain why the visceral muscle cells

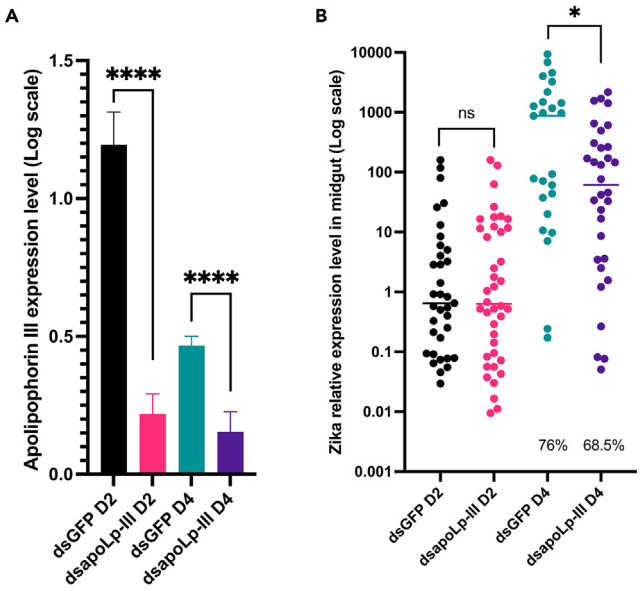

Figure 4. Silencing of *Apolipophorin III* (*apoLP-III*) reduces the Zika virus RNA copy number in the *Ae. aegypti* midgut

(A) Relative expression levels of *apoLP-III* between dsGFP and dsapoLP-III mosquito midguts at 2 days and 4 days post-infection.

(B) Relative expression levels of Zika virus between dsGFP and dsapoLP-III mosquito midguts at 2 days and 4 days post-infection. Double delta Ct analysis was applied, with the value from day 2 dsGFP set as the basal expression level. Day 2: dsGFP $N = 42$, dsapoLP-III $N = 44$. Day 4: dsGFP $N = 29$, dsapoLP-III $N = 32$. The error bar in *apoLP-III* relative expression level represents the standard error of the mean. In Zika virus expression level, the bar indicates the median value and represented on a log scale. Mann-Whitney test was applied for statistical analysis. *$p < 0.05$ ****$p < 0.0001$.

identified in the previous study were not found in our results. Notably, EC emerged as the predominant cell type in the midgut, constituting over 50% in both groups (Table 1). Interestingly, beyond the known cell types, we observed a distinct group of cells that we have named EC-like cells. These cells exhibited a remarkably high expression level of immune-related genes, a phenomenon not previously reported (Figures 1B and S4). The mosquito anterior midgut region, characterized by signs of immune activity and expression of antimicrobial peptides,[40] exhibits similarities to *Drosophila*, where the anterior EC expresses a bacteria defense gene.[6] This collective evidence suggests that this region may be the location of the EC-like cells in the *Ae. aegypti* midgut. In our data, EC-like cells are found to be closer to the ISC/EB cluster but distant from the EC clusters, suggesting that EC-like cells could be in an intermediate phase on the path to becoming mature ECs. However, further experiments are required to elucidate the distribution of each cell type in the mosquito midgut, especially clarifying the role played by less understood cell types, such as EC-like cells.

Our data showed that the ISC/EB proportion is around 20% (Table 1), higher than previously reported percentages of 4.2% in 1-day blood-fed mosquito midgut[7] and 7.5% in *Drosophila* midgut.[6] The physiological changes triggered by blood feeding within the mosquito, such as mechanical distention of the midgut, apoptosis and regeneration of midgut epithelial cells, and altered permeability of the basal lamina,[41–43] might explain the higher ISC/EB percentage observed in our study. Importantly, our study focused on the midgut 4 days post blood feeding, a time point where differentiating cells are highly evident.[41] The subclusters analyzed from ISC/EB revealed a notable abundance of dEB cells, especially in the Zika-infected midgut (Table 2). Epithelial repair is crucial in response to cell loss sustained during viral infection, as viral infection of midgut cells may induce stress and trigger cell signaling responses.[3] The activation of Delta/Notch signaling, crucial in the cellular regenerative program in the midgut, is significant for virus infection.[11] The accelerated turnover of mosquito midgut cells in response to bacterial infection underscores the concordance of our data,[44] particularly the high abundance of dEB in the Zika group. Previous publications also support the idea that the damage might be caused by infection[3,11,42]; therefore, the lower number of cells from the Zika group was able to be performed. Furthermore, the increase in genes related to extracellular matrix remodeling in EE-1 and EC-4 could also illustrate the regeneration of midgut during virus infection (Table S7).

We provide evidence that the virus exists in specific subsets of EC and EE cells, with no presence detected in other cell types (Figure 3). This finding suggests that these two cell types might be the targets for virus infection, given their prominence as major cell types in the midgut. Additionally, the decreased composition of EE-1 with virus infection indicates a potential impact on these cells (Table 1). We acknowledge that the detection of only eleven cells with the virus genome is relatively low, which may be attributed to several reasons. These include the limitations of scRNA-seq, such as its lower sequencing depth and cell capture rate compared to bulk RNA-seq,[45] as well as other potential limitations of the midgut cell isolation preparation. Despite these constraints, the findings presented here are significant, and targeting both EC and EE cells could be crucial in developing strategies to interfere with the virus infection process. Moreover, based on the evidence we have provided, the next step should involve developing a method with stable cell markers, such as fluorescence *in situ* hybridization, to enhance our understanding of the dynamics of virus infection.

ApoLp-III is a hemolymph protein with a crucial role in lipid transport, binding to lipoprotein surfaces and facilitating lipid transport in aqueous media.[32,33] Additionally, apoLp-III emerges as a multifunctional protein, contributing to both humoral and cellular immune responses in various insect species.[46] Furthermore, apoLp-III plays a role in pathogen recognition by binding to various microbial cell walls.[46] Our data reveal a significant upregulation of *apoLp-III* in both the EE-NPF and EE-1 clusters where Zika was detected. In addition to our findings, both *Anopheles gambiae* and *Anopheles stephensi* also exhibit high expression of the ApoLp-III transcript following *Plasmodium* infection in the midgut.[47,48] Therefore, apoLp-III was selected for further functional studies to validate our results. The knockdown experiments showed that apoLp-III impacts the virus RNA copy number at day 4 post-infection in the mosquito midgut (Figure 4), demonstrating that the gene identified as significant from our scRNA-seq results could be a potential target for further investigation. However, no difference was noticed at 2 days post-infection, suggesting that apoLp-III might not affect the virus during the eclipse phase but may impact later when virus starts to replicate. The function of apoLp-III in *Anopheles* depends on the species and strains, exhibiting varying impacts on *Plasmodium*.[47–49] In the context of *Aedes* and Zika virus interactions, apoLp-III may not function as an immune factor against the virus. Instead, it could potentially interfere with virus replication due to its role as a lipid transporter. Given that apoLp-III is a secreted protein, it is likely produced in the EE cells in the midgut, where we observed an increase in transcript levels. However, apoLp-III has demonstrated increased expression in both ovaries and Malpighian tubules after one day of blood feeding in *Anopheles sinensis*[50] and a stable expression level in the carcass in *Anopheles gambiae*, suggesting possible involvement of other tissues during infection. Considering the possible role of apoLp-III, the fat body is worthy to have further investigation. Future experiments should focus on elucidating the interaction between apoLp-III and the virus, understanding how lipid transport or metabolism alters the progression of infection in the gut, and exploring other potential target genes identified in our scRNA-seq results.

In conclusion, our scRNA-seq study has revealed crucial insights into the *Ae. aegypti* mosquito's midgut response to Zika virus infection. Identification of specific cell types, particularly in few subsets of EC and EE, as potencial targets for viral infection, along with the observed upregulation of *apoLp-III* in EE cells, underscores potential key players in the host-virus interaction. Functional studies targeting apoLp-III demonstrated its impact on virus RNA copy numbers, highlighting its significance as a potential target for further investigation. Our findings contribute valuable insights into the cellular and molecular dynamics of mosquito midguts during Zika virus infection, offering potential avenues for developing strategies to combat mosquito-borne viral diseases.

Limitations of the study

Although *Aedes aegypti* is a critical vector for viruses, the resources, techniques, and references are limited. We acknowledge that the number of cells detected with the virus genome is relatively low, possibly due to the limitations of scRNA-seq, which has lower sequencing depth and cell capture rate compared to bulk RNA-seq. The other possible reason is the cell recovery rate is only approximately 20%, taking into account that the mosquito midgut is estimated to have around 500 endocrine cells.[51] A previous study utilizing the single nuclei isolation method also reported a low recovery rate of 30%,[7] indicating the challenge of recovering most of the cells from the midgut. Additionally, another possibility could be that the isolation method involved in density gradient separation removed apoptotic cells caused by virus infection.[52] We explored alternative methods, including Ficoll-Paque PLUS density gradient media and Histopaque-1119, but found Optiprep to be the most effective choice. Furthermore, we experimented with various enzymes aside from elastase, such as collagenase and dispase, as well as combinations of all three, yet elastase yielded the best outcome. The data and techniques we provided are important to show the successful isolation of midgut cells and the first detection of the virus genome in certain cell types. The lack of cell sorting techniques for separating different cell types for further validation is another limitation. However, this study, with our findings, is an important step toward understanding mosquito-virus interactions.

STAR★METHODS

Detailed methods are provided in the online version of this paper and include the following:

- KEY RESOURCES TABLE
- RESOURCE AVAILABILITY
  - Lead contact
  - Materials availability
  - Data and code availability
- EXPERIMENTAL MODEL AND STUDY PARTICIPANT DETAILS
  - Mosquitoes
  - Mouse
- METHOD DETAILS
  - Virus preparation and *Ae. aegypti* infection
  - Single-cell suspension preparation
  - High-throughput sequencing
  - scRNA-Seq data analyzing
  - Differential gene expression analysis during virus infection

○ Gene silencing in *Ae. aegypti*
● QUANTIFICATION AND STATISTICAL ANALYSIS

SUPPLEMENTAL INFORMATION

Supplemental information can be found online at https://doi.org/10.1016/j.isci.2024.110353.

ACKNOWLEDGMENTS

We thank Dr. Guilin Wang and Dr. Dejian Zhao from YGCA for their invaluable advice on sample preparation. This work was supported in part by the NIH (AI52904) and the Howard Hughes Medical Institute Emerging Pathogens Initiative.

AUTHOR CONTRIBUTIONS

T.-Y.C., H.R., A.M.L., Y.C., and E.F. conceived and designed the experiments. T.-Y.C., H.R., and A.M.L. performed the experiments. T-Y.C. and Y.C. analyzed the data. T.-Y.C. and E.F. wrote the manuscript with contributions from all authors. All authors have approved the final version of the manuscript.

DECLARATION OF INTERESTS

The authors declare no competing interests.

DECLARATION OF GENERATIVE AI AND AI-ASSISTED TECHNOLOGIES IN THE WRITING PROCESS

During the preparation of this work, the authors used ChatGPT and Grammarly to ensure there were no grammar issues. After using these tools, the authors reviewed and edited the content as needed and take full responsibility for the content of the publication.

Received: April 10, 2024
Revised: May 21, 2024
Accepted: June 20, 2024
Published: June 22, 2024

REFERENCES

1. Billingsley, P.F. (1990). The midgut ultrastructure of hematophagous insects. Annu. Rev. Entomol. *35*, 219–248. https://doi.org/10.1146/annurev.en.35.010190.001251.
2. Lehane, M., and Billingsley, P. (1996). Biology of the Insect Midgut (Springer Science), pp. 151–320.
3. Hixson, B., Taracena, M.L., and Buchon, N. (2021). Midgut epithelial dynamics are central to mosquitoes' physiology and fitness, and to the transmission of vector-borne disease. Front. Cell. Infect. Microbiol. *11*, 653156.
4. Franz, A.W.E., Kantor, A.M., Passarelli, A.L., and Clem, R.J. (2015). Tissue barriers to arbovirus infection in mosquitoes. Viruses *7*, 3741–3767. https://doi.org/10.3390/v7072795.
5. Severson, D.W., and Behura, S.K. (2016). Genome investigations of vector competence in *Aedes aegypti* to inform novel arbovirus disease control approaches. Insects *7*, 58. https://doi.org/10.3390/insects7040058.
6. Hung, R.-J., Hu, Y., Kirchner, R., Liu, Y., Xu, C., Comjean, A., Tattikota, S.G., Li, F., Song, W., Ho Sui, S., and Perrimon, N. (2020). A cell atlas of the adult Drosophila midgut. Proc. Natl. Acad. Sci. USA *117*, 1514–1523. https://doi.org/10.1073/pnas.1916820117.
7. Cui, Y., and Franz, A.W.E. (2020). Heterogeneity of midgut cells and their differential responses to blood meal ingestion by the mosquito, Aedes aegypti. Insect Biochem. Mol. Biol. *127*, 103496. https://doi.org/10.1016/j.ibmb.2020.103496.
8. Jiang, H., Patel, P.H., Kohlmaier, A., Grenley, M.O., McEwen, D.G., and Edgar, B.A. (2009). Cytokine/Jak/Stat signaling mediates regeneration and homeostasis in the Drosophila midgut. Cell *137*, 1343–1355. https://doi.org/10.1016/j.cell.2009.05.014.
9. Ren, F., Wang, B., Yue, T., Yun, E.-Y., Ip, Y.T., and Jiang, J. (2010). Hippo signaling regulates Drosophila intestine stem cell proliferation through multiple pathways. Proc. Natl. Acad. Sci. USA *107*, 21064–21069. https://doi.org/10.1073/pnas.1012759107.
10. Jiang, H., Grenley, M.O., Bravo, M.-J., Blumhagen, R.Z., and Edgar, B.A. (2011). EGFR/Ras/MAPK signaling mediates adult midgut epithelial homeostasis and regeneration in Drosophila. Cell Stem Cell *8*, 84–95. https://doi.org/10.1016/j.stem.2010.11.026.
11. Taracena, M.L., Bottino-Rojas, V., Talyuli, O.A.C., Walter-Nuno, A.B., Oliveira, J.H.M., Angleró-Rodriguez, Y.I., Wells, M.B., Dimopoulos, G., Oliveira, P.L., and Paiva-Silva, G.O. (2018). Regulation of midgut cell proliferation impacts *Aedes aegypti* susceptibility to dengue virus. PLoS Negl. Trop. Dis. *12*, e0006498. https://doi.org/10.1371/journal.pntd.0006498.
12. Ohlstein, B., and Spradling, A. (2007). Multipotent Drosophila intestinal stem cells specify daughter cell fates by differential Notch signaling. Science *315*, 988–992. https://doi.org/10.1126/science.1136606.
13. Ohlstein, B., and Spradling, A. (2006). The adult Drosophila posterior midgut is maintained by pluripotent stem cells. Nature *439*, 470–474. https://doi.org/10.1038/nature04333.
14. Perdigoto, C.N., Schweisguth, F., and Bardin, A.J. (2011). Distinct levels of Notch activity for commitment and terminal differentiation of stem cells in the adult fly intestine. Development *138*, 4585–4595. https://doi.org/10.1242/dev.065292.
15. Jiang, H., and Edgar, B.A. (2012). Intestinal stem cell function in Drosophila and mice. Curr. Opin. Genet. Dev. *22*, 354–360. https://doi.org/10.1016/j.gde.2012.04.002.
16. Korzelius, J., Naumann, S.K., Loza-Coll, M.A., Chan, J.S., Dutta, D., Oberheim, J., Gläßer, C., Southall, T.D., Brand, A.H., Jones, D.L., and Edgar, B.A. (2014). Escargot maintains stemness and suppresses differentiation in Drosophila intestinal stem cells. EMBO J. *33*, 2967–2982. https://doi.org/10.15252/embj.201489072.
17. Korzelius, J., Azami, S., Ronnen-Oron, T., Koch, P., Baldauf, M., Meier, E., Rodriguez-Fernandez, I.A., Groth, M., Sousa-Victor, P., and Jasper, H. (2019). The WT1-like transcription factor Klumpfuss maintains lineage commitment of enterocyte progenitors in the Drosophila intestine. Nat. Commun. *10*, 4123. https://doi.org/10.1038/s41467-019-12003-0.
18. Lee, W.-C., Beebe, K., Sudmeier, L., and Micchelli, C.A. (2009). Adenomatous polyposis coli regulates Drosophilaintestinal stem cell proliferation. Development *136*, 2255–2264. https://doi.org/10.1242/dev.035196.

19. Mathur, D., Bost, A., Driver, I., and Ohlstein, B. (2010). A transient niche regulates the specification of Drosophila intestinal stem cells. Science *327*, 210–213. https://doi.org/10.1126/science.1181958.
20. Zeng, X., and Hou, S.X. (2015). Enteroendocrine cells are generated from stem cells through a distinct progenitor in the adult Drosophila posterior midgut. Development *142*, 644–653. https://doi.org/10.1242/dev.113357.
21. Brown, M.R., Crim, J.W., Arata, R.C., Cai, H.N., Chun, C., and Shen, P. (1999). Identification of a Drosophila brain-gut peptide related to the neuropeptide Y family. Peptides *20*, 1035–1042. https://doi.org/10.1016/S0196-9781(99)00097-2.
22. Veenstra, J.A., Noriega, F.G., Graf, R., and Feyereisen, R. (1997). Identification of three Allatostatins and their cDNA from the mosquito *Aedes aegypti*. Peptides *18*, 937–942. https://doi.org/10.1016/S0196-9781(97)00032-6.
23. Nässel, D.R., Zandawala, M., Kawada, T., and Satake, H. (2019). Tachykinins: neuropeptides that are ancient, diverse, widespread and functionally pleiotropic. Front. Neurosci. *13*, 1262.
24. Predel, R., Neupert, S., Garczynski, S.F., Crim, J.W., Brown, M.R., Russell, W.K., Kahnt, J., Russell, D.H., and Nachman, R.J. (2010). Neuropeptidomics of the mosquito *Aedes aegypti*. J. Proteome Res. *9*, 2006–2015. https://doi.org/10.1021/pr901187p.
25. Park, J.-H., and Kwon, J.Y. (2011). Heterogeneous Expression of Drosophila Gustatory Receptors in Enteroendocrine Cells. PLoS One *6*, e29022. https://doi.org/10.1371/journal.pone.0029022.
26. Hwang, B., Lee, J.H., and Bang, D. (2018). Single-cell RNA sequencing technologies and bioinformaticspipelines. Exp. Mol. Med. *50*, 1–14. https://doi.org/10.1038/s12276-018-0071-8.
27. Salazar, M.I., Richardson, J.H., Sánchez-Vargas, I., Olson, K.E., and Beaty, B.J. (2007). Dengue virus type 2: replication and tropisms in orally infected *Aedes aegypti* mosquitoes. BMC Microbiol. *7*, 9. https://doi.org/10.1186/1471-2180-7-9.
28. Reimand, J., Arak, T., Adler, P., Kolberg, L., Reisberg, S., Peterson, H., and Vilo, J. (2016). g:Profiler—a web server for functional interpretation of gene lists (2016 update). Nucleic Acids Res. *44*, W83–W89. https://doi.org/10.1093/nar/gkw199.
29. Supek, F., Bošnjak, M., Škunca, N., and Šmuc, T. (2011). REVIGO summarizes and visualizes long lists of gene ontology terms. PLoS One *6*, e21800. https://doi.org/10.1371/journal.pone.0021800.
30. Vadnal, R., and Parthasarathy, R. (1995). Myo-inositol monophosphatase: diverse effects of lithium, carbamazepine, and valproate. Neuropsychopharmacology *12*, 277–285. https://doi.org/10.1016/0893-133X(94)00088-H.
31. Sieglaff, D.H., Duncan, K.A., and Brown, M.R. (2005). Expression of genes encoding proteins involved in ecdysteroidogenesis in the female mosquito, *Aedes aegypti*. Insect Biochem. Mol. Biol. *35*, 471–490. https://doi.org/10.1016/j.ibmb.2005.01.011.
32. Van der Horst, D.J., Weers, P.M., and Van Marrewijk, W.J. (1993). Lipoproteins and lipid transport. In Insect Lipids: Chemistry, Biochemistry & Biology, D.W. Santely-samuelson and D.R. Nelson, eds. (University of Nebraska Press), pp. 1–24.
33. Blacklock, B.J., and Ryan, R.O. (1994). Hemolymph lipid transport. Insect Biochem. Mol. Biol. *24*, 855–873.
34. Kantor, A.M., Dong, S., Held, N.L., Ishimwe, E., Passarelli, A.L., Clem, R.J., and Franz, A.W.E. (2017). Identification and initial characterization of matrix metalloproteinases in the yellow fever mosquito, Aedes aegypti. Insect Mol. Biol. *26*, 113–126. https://doi.org/10.1111/imb.12275.
35. Timpl, R., Sasaki, T., Kostka, G., and Chu, M.-L. (2003). Fibulins: a versatile family of extracellular matrix proteins. Nat. Rev. Mol. Cell Biol. *4*, 479–489. https://doi.org/10.1038/nrm1130.
36. Jansen, E., Ayoubi, T.A., Meulemans, S.M., and Van de Ven, W.J. (1995). Neuroendocrine-specific expression of the human prohormone convertase 1 gene: hormonal regulation of transcription through distinct cAMP response elements. J. Biol. Chem. *270*, 15391–15397. https://doi.org/10.1074/jbc.270.25.15391.
37. Behura, S.K., Gomez-Machorro, C., Harker, B.W., deBruyn, B., Lovin, D.D., Hemme, R.R., Mori, A., Romero-Severson, J., and Severson, D.W. (2011). Global cross-talk of genes of the mosquito *Aedes aegypti* in response to dengue virus infection. PLoS Negl. Trop. Dis. *5*, e1385. https://doi.org/10.1371/journal.pntd.0001385.
38. Colpitts, T.M., Cox, J., Vanlandingham, D.L., Feitosa, F.M., Cheng, G., Kurscheid, S., Wang, P., Krishnan, M.N., Higgs, S., and Fikrig, E. (2011). Alterations in the *Aedes aegypti* transcriptome during infection with West Nile, dengue and yellow fever viruses. PLoS Pathog. *7*, e1002189. https://doi.org/10.1371/journal.ppat.1002189.
39. Chen, T.-Y., Lee, Y., Wang, X., Mathias, D., Caragata, E.P., and Smartt, C.T. (2021). Profiling transcriptional response of dengue-2 virus infection in midgut tissue of *Aedes aegypti*. Front. Trop. Dis. *2*, 708817. https://doi.org/10.3389/fitd.2021.708817.
40. Hixson, B., Bing, X.-L., Yang, X., Bonfini, A., Nagy, P., and Buchon, N. (2022). A transcriptomic atlas of Aedes aegypti reveals detailed functional organization of major body parts and gut regional specializations in sugar-fed and blood-fed adult females. Elife *11*, e76132. https://doi.org/10.7554/eLife.76132.
41. Okuda, K., de Almeida, F., Mortara, R.A., Krieger, H., Marinotti, O., and Bijovsky, A.T. (2007). Cell death and regeneration in the midgut of the mosquito, *Culex quinquefasciatus*. J. Insect Physiol. *53*, 1307–1315. https://doi.org/10.1016/j.jinsphys.2007.07.005.
42. Dong, S., Balaraman, V., Kantor, A.M., Lin, J., Grant, D.G., Held, N.L., and Franz, A.W.E. (2017). Chikungunya virus dissemination from the midgut of *Aedes aegypti* is associated with temporal basal lamina degradation during bloodmeal digestion. PLoS Negl. Trop. Dis. *11*, e0005976. https://doi.org/10.1371/journal.pntd.0005976.
43. Kantor, A.M., Grant, D.G., Balaraman, V., White, T.A., and Franz, A.W.E. (2018). Ultrastructural Analysis of Chikungunya Virus Dissemination from the Midgut of the Yellow Fever Mosquito, *Aedes aegypti*. Viruses *10*, 571. https://doi.org/10.3390/v10100571.
44. Taracena-Agarwal, M.L., Hixson, B., Nandakumar, S., Girard-Mejia, A.P., Chen, R.Y., Huot, L., Padilla, N., and Buchon, N. (2024). The midgut epithelium of mosquitoes adjusts cell proliferation and endoreplication to respond to physiological challenges. BMC Biol. *22*, 22.
45. Chang, J.-T., Liu, L.-B., Wang, P.-G., and An, J. (2024). Single-cell RNA sequencing to understand host-virus interactions. Virol. Sin. *39*, 1–8. https://doi.org/10.1016/j.virs.2023.11.009.
46. Zdybicka-Barabas, A., and Cytryńska, M. (2013). Apolipophorins and insects immune response. Invertebr. Surviv. J. *10*, 58–68.
47. Gupta, L., Noh, J.Y., Jo, Y.H., Oh, S.H., Kumar, S., Noh, M.Y., Lee, Y.S., Cha, S.-J., Seo, S.J., Kim, I., et al. (2010). Apolipophorin-III mediates antiplasmodial epithelial responses in *Anopheles gambiae* (G3) mosquitoes. PLoS One *5*, e15410.
48. Dhawan, R., Gupta, K., Kajla, M., Kakani, P., Choudhury, T.P., Kumar, S., Kumar, V., and Gupta, L. (2017). Apolipophorin-III acts as a positive regulator of Plasmodium development in *Anopheles stephensi*. Front. Physiol. *8*, 185.
49. Mendes, A.M., Schlegelmilch, T., Cohuet, A., Awono-Ambene, P., De Iorio, M., Fontenille, D., Morlais, I., Christophides, G.K., Kafatos, F.C., and Vlachou, D. (2008). Conserved mosquito/parasite interactions affect development of Plasmodium falciparum in Africa. PLoS Pathog. *4*, e1000069.
50. NOH, M.Y., Won, R., JO, Y.H., LEE, Y.S., and HAN, Y.S. (2009). Cloning and blood-meal dependent induction pattern of apolipophorin-III from *Anopheles sinensis*. Entomol. Res. *39*, 388–393.
51. Brown, M.R., Raikhel, A.S., and Lea, A.O. (1985). Ultrastructure of midgut endocrine cells in the adult mosquito, *Aedes aegypti*. Tissue Cell *17*, 709–721.
52. Ayers, J.B., Coatsworth, H.G., Kang, S., Dinglasan, R.R., and Zhou, L. (2021). Clustered rapid induction of apoptosis limits ZIKV and DENV-2 proliferation in the midguts of *Aedes aegypti*. Commun. Biol. *4*, 69. https://doi.org/10.1038/s42003-020-01614-9.
53. Uraki, R., Hastings, A.K., Gloria-Soria, A., Powell, J.R., and Fikrig, E. (2018). Altered vector competence in an experimental mosquito-mouse transmission model of Zika infection. PLoS Negl. Trop. Dis. *12*, e0006350.
54. Hao, Y., Hao, S., Andersen-Nissen, E., Mauck, W.M., Zheng, S., Butler, A., Lee, M.J., Wilk, A.J., Darby, C., Zager, M., et al. (2021). Integrated analysis of multimodal single-cell data. Cell *184*, 3573–3587.e29. https://doi.org/10.1016/j.cell.2021.04.048.

STAR★METHODS

KEY RESOURCES TABLE

REAGENT or RESOURCE	SOURCE	IDENTIFIER
Biological sample		
Aedes aegypti: Orlando strain	Dr. Erol Fikrig Laboratory[53]	N/A
Mus musculus: AG129: Ifnαr1-/-Ifnγr-/-	Dr. Erol Fikrig Laboratory[53]	N/A
Zika virus MEX2-81 strain	Dr. Erol Fikrig Laboratory[53]	N/A
C6/36 cells	ATCC	Cat# CRL-1660
BHK-21 cells	ATCC	Cat# CCL-10
Peptides and chemicals		
Oligonucleotides	The Keck Oligonucleotide Synthesis facility	See Table S1
Elastase	Sigma-Aldrich	Cat# E0258
OptiPrep densist gradient medium	Sigma-Aldrich	Cat# D1556
Chromium Next GEM Single Cell 5′ GEM Kit v2	10x Genomics	www.10xgenomics.com
TranscriptAid T7 High Yield Transcription Kit	Thermo Scientific	Cat# K0441
Deposited data		
Aedes aegypti midgut scRNA-seq data	This paper	GSE267972
Aedes aegypti LVP_AGWG AaegL5 chromosome and transcripts	VectorBase	www.vectorbase.org/
Zika virus genome	NCBI	www.ncbi.nlm.nih.gov/
Software and algorithms		
Cell Ranger v7.1.0	10x Genomics	www.10xgenomics.com
RStudio v2023.060.0+421	The R Project	www.r-project.org
Seurat v4.3.0	Hao et al.	cran.rproject.org/web/packages/Seurat/index.html
Prism v10	GraphPad	www.graphpad.com/

RESOURCE AVAILABILITY

Lead contact

Further information and requests for resources and reagents should be directed to and will be fulfilled by the lead contact, Tse-Yu Chen (tse-yu.chen@yale.edu).

Materials availability

This study did not generate new unique reagents.

Data and code availability

Single-cell RNA-seq data have been deposited at Gene Expression Omnibus and are publicly available as of the date of publication. Accession numbers are listed in the key resources table.

No original code has been used in this paper.

Any additional information required to reanalyze the data reported in this paper is available from the lead contact upon request.

EXPERIMENTAL MODEL AND STUDY PARTICIPANT DETAILS

Mosquitoes

The *Ae. aegypti* (Orlando strain) mosquitoes were maintained in a climate-controlled room at 28°C with a relative humidity ranging between 60–80%, following a light: dark cycle of 14:10 h. Upon hatching, larvae were separated into pans at an approximate density of 200 larvae per pan and were provided with fish food (WardleyAquatics). Adult mosquitoes had *ad libitum* access to cotton rolls soaked in a 10% sucrose solution. The mosquito colonies were sustained by feeding female mosquitoes on blood sourced from naïve AG129 mice (IACUC202110404).

Mouse

Eight- to twelve-week-old Ifnαr1-/-Ifnγr-/- mice (AG129 –SV129 background) were used in this study. Mice were bred in a specific-pathogen-free facility at Yale University.

METHOD DETAILS

Virus preparation and *Ae. aegypti* infection

The Zika virus (MEX2-81 strain) was cultivated in *Aedes albopictus* C6/36 cells, which were cultured in Dulbecco modified Eagle medium (DMEM)(Gibco) supplemented with 10% fetal bovine serum (FBS) and 1% penicillin/streptomycin (Invitrogen). The cell cultures were maintained at 30°C with 5% CO_2.

The plaque assay was employed to determine the virus titer. BHK-21 cells were cultured in DMEM supplemented with 10% FBS and 1% penicillin/streptomycin at 37°C with 5% CO_2. The cells were seeded into a 24-well plate and incubated with a series of diluted virus samples for 1 hour. Following incubation, an overlayer medium (DMEM with 2% FBS, 2% carboxymethylcellulose, and 1% penicillin/streptomycin) was added to each well and cultured for 5 days. To fix the plate, a 10% formaldehyde solution was added to each well and incubated for 1 hour. Subsequently, the solution in the plate was discarded, and staining solution (crystal violet 5g, methanol 400ml, and ddH_2O 100ml) was added for incubation 2 hours. After washing, plaques were counted to calculate the plaque-forming units (PFU).

Female *Ae. aegypti*, aged 4–7 days, were divided into two groups: the control group and the Zika group. The control group was fed on a naïve AG129 mouse, while the Zika group was fed on a mouse infected with Zika virus. The Zika-infected AG129 mouse received a subcutaneous injection of 100 PFU of Zika virus three days before exposure to the mosquitoes. The Zika-infected AG129 mouse exhibited a viral load of 4.6 log PFU/ml. Following a half-hour feeding period, the engorged females were collected into new containers and provided with 10% sucrose solution *ad libitum*.

Single-cell suspension preparation

Female mosquito midguts were dissected after 4 days of either blood feeding or infection. Each midgut was finely chopped into small pieces using a needle (BD PrecisionGlide Needle 27G x 1/2) and immediately transferred into an Eppendorf tube containing 200 μl of cold Schneider's Drosophila Medium with 0.2 mM ethylenediaminetetraacetic acid (EDTA) to minimize exposure to room temperature. A total of fifty midguts from each group were collected and incubated with 200 μl of a 2 mg/ml elastase/PBS solution (Sigma-Aldrich) on a shaker at 37°C for 30 minutes. To halt the digestion reaction and prevent cell aggregation, 400 μl of 2% bovine serum albumin (BSA) in PBS was added. The cell suspension was then passed through a 40 μm cell strainer (SP Bel-art) and loaded onto the top of an Optiprep (Axis-Shield) density gradient with a density of 1.216 g/ml. Viable cells were isolated from the top layer of the sample after centrifugation at 800g for 20 minutes. Cell viability and count were determined through 0.4% trypan blue staining and cell counting using a hemocytometer. The cells were concentrated with an 800g centrifuge for 5 minutes to remove excess liquid. A final volume of 35 μl single-cell mix was promptly submitted to the Yale Keck Microarray Shared Resource (KMSR) with a concentration of 235 cells/μl in the control group and 449 cells/μl in the Zika group.

Reverse transcription and library preparation were conducted at KMSR using the Chromium Next GEM Single Cell 5' GEM Kit v2. Both poly-dT primer and the Zika virus NS5 RT primer (Table S1) were employed in the generation of the cDNA library, facilitating subsequent processing with the 10x Genomics.

High-throughput sequencing

The library concentration passed quality control, showing a viability of 95%. The library concentrations were measured at 57 ng/μl in the control group and 68.5 ng/μl in the Zika group, with an average fragment size of 476 base pairs in the control and 455 base pairs in the Zika group. These results meet the criteria for sequencing at the Yale Center for Genome Analysis (YCGA). The NovaSeq instrument was utilized for sequencing, following the specifications for the 10X Single Cell 5 Prime sample type, with a reading length of HS4000 150bp paired-end.

scRNA-Seq data analyzing

Cell Ranger (version 7.1.0) was used for the initial data analysis at KMSR. In summary, the analysis included demultiplexing, collapsing unique molecular identifiers (UMIs), and aligning the data to the *Ae. aegypti* LVP_AGWG AaegL5 chromosome and transcripts reference files, accessible on VectorBase (https://vectorbase.org/). Additionally, alignment to the Zika virus genome obtained from the National Center for Biotechnology Information (NCBI) was conducted as part of the comprehensive analysis.

The raw data produced by Cell Ranger was imported into the R toolkit Seurat (version 4.3.0) for comparative analysis of scRNA-Seq datasets.[54] Cells with a gene count of less than 100 were excluded from the analysis and considered as damaged cells. The LogNormalize method was applied to normalize gene transcription measurements for each cell based on its total transcript count. To integrate the datasets of Control and Zika midguts, the FindIntegrationAnchors function was utilized to identify anchors, and these anchors were employed in the IntegrateData function for dataset integration, using the default method for clustering. The dimensionality of the data was reduced through Uniform Manifold Approximation and Projection (UMAP) for single-cell data visualization. Applying FindClusters with a resolution parameter of 1 facilitated cell clustering. To identify canonical cell type marker genes conserved in both Control and Zika midguts, the FindConservedMarkers function was employed. Visualization of conserved cell type markers across conditions, indicating both expression

levels and the percentage of cells in a cluster expressing a given gene, was achieved using the DotPlot function, with the inclusion of the split-by parameter.

Differential gene expression analysis during virus infection

The Seurat function FindMarkers was utilized to detect genes with differential expression (fold-change ≥ 2 or ≤ -2 and adjusted p-value <0.05) in midguts between the Control and Zika groups. To visually represent the gene expression alterations triggered by virus infection, the Seurat functions FeaturePlot and VlnPlot were employed. Statistical analyses of significance levels pertaining to both gene expression levels and cell proportions within each cluster, comparing midguts from the Control and Zika groups, were conducted using the Wilcoxon signed-rank test.

Gene silencing in *Ae. aegypti*

Double-strand RNA (dsRNA) was designed to target either *GFP* or *apoLP-III*. The dsRNA template was generated through Polymerase Chain Reaction (PCR). The reaction followed the protocol of Phusion High-Fidelity DNA Polymerase (New England Biolabs), utilizing 400 μg of *Ae. aegypti* cDNA library or GFP plasmid in a 200 μl reaction with primers containing the T7 sequence (Table S1). PCR conditions included 1 cycle of 98°C for 30 s, followed by 40 cycles of 98°C for 10 s, 55°C for 30 s, and 72°C for 30 s, capped by 1 cycle of 72°C for 5 min. Subsequently, PCR products were purified using the Monarch DNA Gel Extraction Kit (New England Biolabs). The template then used for dsRNA synthesis was generated using the TranscriptAid T7 High Yield Transcription Kit (Thermo Scientific). The reaction involved a four-hour incubation at 37°C, followed by the purification of RNA transcripts according to the manufacturer's protocol. The dsRNA concentration was measured using NanoDrop 2000C Spectrophotometers (Thermo Scientific).

Four to seven days old female *Ae. aegypti* were microinjected with 500 ng of dsGFP or dsapoLP-III using the Nanoject II Auto-Nanoliter Injector (Drummond Scientific). After 3 days post-injection, both dsGFP and dsapoLP-III groups were exposed to the same Zika virus-infected AG129 mice following the same procedure described earlier. The average viral titer in the Zika-infected AG129 mice was 4.56 ± 0.36 log PFU/ml from replicate experiments. The midgut was dissected after 2- and 4-days of infection, and individual midgut RNA was extracted using NucleoSpin RNA Columns (Takara Bio). The cDNA was generated with the iScript™ cDNA Synthesis Kit (Bio-Rad), and Real-time PCR was used to quantify the virus and *apoLP-III* expression levels with the reference gene RP49 (Table S1). The virus RNA copy number and gene expression were determined by assessing the Ct (cycle threshold) value normalized to RP49. Double delta Ct analysis was applied, with the value from day 2 dsGFP set as the basal expression level. The statistics were calculated using Mann-Whitney test with GraphPad Prism software (Prism 10) to compare between dsGFP and dsapoLP-III infected mosquito groups.

QUANTIFICATION AND STATISTICAL ANALYSIS

The statistical methods used are related to the bioinformatics analyses of the data and are fully described in the above sections. The bioinformatics functions and their parameters are listed in the above sections. The significance threshold level was set to $p < 0.05$.